Available online at www.sciencedirect.com
SCIENCE DIRECT®
Journal of Nuclear Materials 328 (2004) 31–45
journal of nuclear materials
www.elsevier.com/locate/jnucmat

Contribution to the understanding of the ZrNb(l%)O(0.13%) oxidation mechanism at 500 °C in dry air

J.J. Vermoyal [a,*], A. Frichet [b], L. Dessemond [c]

[a] CEZUS Research Center, rue Paul Girod, 73403 Ugine, France
[b] Framatome ANP Nuclear Fuel, 10 rue Juliette Récamier, 69006 Lyon, France
[c] Laboratory of Electrochemistry and Physical-Chemistry of Materials and Interfaces, UMR 5631 INPG-CNRS-UJ, 38402 Saint Martin d'Hères, France

Received 28 August 2003; accepted 26 February 2004

Abstract

The oxidation of ZrNb(l%)O(0.13%) at 500 °C in dry air was investigated in situ by thermogravimetric analyses and electrochemical impedance spectroscopy. Sheets of the alloy were coated with different noble metals (Pt, Au, Ag) as electrode material. After an initial sub-parabolic rate law, the kinetics of ZrNb(l%)O(0.13%) oxidation are characterized by a transition to another decreasing rate law for different times and thicknesses. Noble metals were observed to clearly modify the oxidation rate, even when a pre-oxidized zirconia film was formed before the deposit and the increase in the oxidation rate was always monitored for thick oxides (30 μm). The kinetic transition is hypothesized to be associated with the microstructural degradation of the oxide film. Localized oxidation rate increases were revealed by scanning electron microscopy at the tip of radial cracks distributed on more than 2% of the total area of the sample. Catalytic effects observed on the oxidation rate after the noble metal deposition suggest that the mechanism controlling the oxidation rate is not a solely one of oxygen diffusion through the oxide layer. The reaction of oxygen reduction at the oxide/metal/gas interface partially controls the oxidation kinetics of ZrNb(l%)O(0.13%). Complex electrical signatures monitored during the oxide growth corroborate this assumption and hence indicate that oxygen reduction is still partially controlling the oxidation rate when noble metal are present on ZrNb(l%)O(0.13%) surface. Finally, a mixed process of interfacial-diffusion mechanism is proposed to be the rate determining step for ZrNb(l%)O(0.13%) oxidation in this environment.

1. Introduction

The purpose of this study was to gain some insight into the mechanism of ZrNb(l%)O(0.13%) oxidation using information recorded in situ during the oxide growth using two techniques: thermogravimetric analysis (TGA) for weight gain measurements and electrochemical impedance spectroscopy (EIS) for electrical properties associated with the oxide film formation.

The thermal oxidation of zirconium alloys is generally described by an initial cubic or parabolic pre-transition stage followed by a quasi linear variation law [1,2]. Since oxide film is only produced by oxygen vacancy diffusion [3] (cationic transport number is negligible in zirconia film), previous work carried out on Zircaloy-4 (Zr alloy containing Sn(1.3%), Fe(0.2%), Cr(0.1%)) had shown that platinum could be used as an electrode material deposited on ZrO_2 surface in order to follow in situ the oxidation process [4]. Results of the literature show that the coating of a noble metal on the electrochemical reaction sites (ERS) of oxygen reduction (generally assumed to be localized at the oxide/gas interface) may modify the oxidation rate if the

* Corresponding author. Fax: +33-4 7989 3864.
E-mail address: jean-jerome.vermoyal@framatome-anp.com (J.J. Vermoyal).

0022-3115/$ - see front matter © 2004 Elsevier B.V. All rights reserved.
doi:10.1016/j.jnucmat.2004.02.013

determining step involves this interfacial process (see for instance in Ref. [4]). In the case of Zircaloy-4 (Zy-4), no difference in the kinetics behaviour could be seen between the Pt-coated and the uncoated specimen. Owing to the constant thickness of the dense oxide layer determined by EIS in situ investigations, we thus concluded that the oxygen diffusion through the oxide layer was the rate determining oxidation step [4].

The influence of the oxygen reduction kinetics at the ZrO_2/gas interface on the oxidation rate of ZrNb(l%)O(0.13%) is likely to be studied by changing the nature of the noble metal. During the oxidation of Zr alloys, electrons are injected at the metal/oxide interface and move through the oxide layer toward the ERS. This is quite different from solid electrolyte. In the latter case, electrons engaged in the reduction reaction are only provided from the electrode material. In the present work, the presence of a noble metal at the ZrO_2/gas interface and the properties of each electrode material could then interfere with the oxide growth rate if the interfacial oxygen reduction process is the kinetic determining step of the ZrNb(l%)O(0.13%) oxidation (or one of the determining step in case of a multiple steps mechanism).

2. Experimental

The chemical composition of the sheets of ZrNb(l%)O(0.13%) provided by Cezus (France) is listed in Table 1. The size of the β-Nb precipitates size was estimated to be around 50 nm. For the sake of simplicity, the samples studied will be referenced as ZrNbO in the following. Both weight gain experiments and electrochemical characterizations are described in detail elsewhere [4]. TGA and EIS experiments were performed in the same oxidation conditions (500 °C, dry air) but in separated devices. Noble metals (Pt, Ag and Au) were deposited on ZrNbO by RF sputtering at room temperature [5]. In most cases (see in the text), samples were pre-oxidized (oxide thickness of 1.1 ± 0.2 μm) at 500 °C in dry air before metal coating (without grid contact) in order to avoid any modification of the ZrO_2 properties such as microstructure or oxidation resistance, by possible formation of 'ZrNbO-noble metal' intermetallic layer. Four EIS studies were carried out on a ZrNbO/ZrO_2/Pt cell (Fig. 1) but only one with an Au electrode because of its degradation at 500 °C (and for silver deposit too, see below for further explanations). The dimensions of the Pt grid are 0.2 mm for the thickness and 1.5 mm for the mesh. Linear sweep voltamograms were recorded during oxidation at a scan rate of 2 $mV\,min^{-1}$ using a potentiostat–galvanostat (Radiometer PGS201T).

3. Results

3.1. Oxidation kinetics

A typical oxidation kinetic curve for as-fabricated ZrNbO is characterized by two consecutive sub-parabolic rate laws (Fig. 2). After 120 h of isothermal treatment corresponding to an oxide thickness close to 7–8 μm, the oxidation rate progressively increases before the beginning of a new sub-parabolic rate law. Generally, the oxide thicknesses (or the weight gain due to oxidation) can be expressed as a power, m, of the oxidation time t, according to the following equation:

$$S = kt^m, \tag{1}$$

where k is the rate constant, and m is equal to 1/2 or 1/3 for parabolic and cubic behaviours respectively. Exper-

Table 1
Chemical composition of the ZrNbO sheets

Element	Nb	Fe	C	O	Si
Wt%	1.0	0.009	0.0027	0.128	<0.001

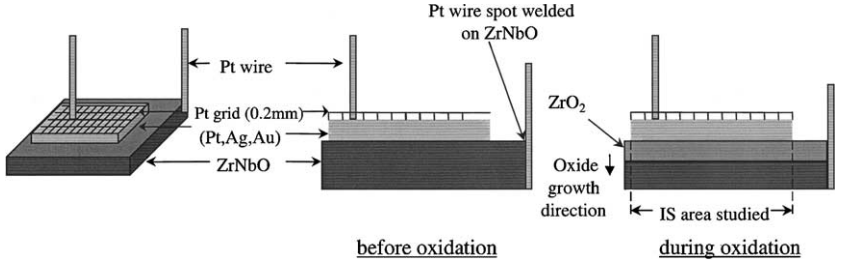

Fig. 1. Scheme of the electrochemical cell.

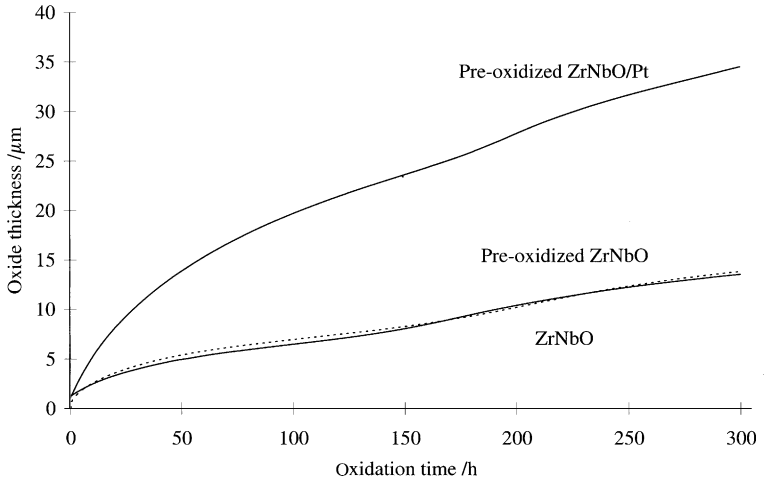

Fig. 2. Oxide thickness versus time determined by TGA for ZrNbO (dashed line), pre-oxidized ZrNbO (see text for detail-full line) and pre-oxidized ZrNbO coated with Pt.

Table 2
Kinetic parameters for ZrNbO, uncoated and coated samples, pre-oxidized and non-pre-oxidized, time and oxide thickness at the transition determined by TGA (and SEM for oxide thickness)

	Pre-transition		Transition		Oxide thickness after 300 h (μm)	
	$k/\mu m\,h^{-1}$	m	Time (h)	Oxide thickness (μm)	TGA	SEM
Reference[a]	1.0 ± 0.2	0.43 ± 0.05	120 ± 10	7.8 ± 0.1	14.1 ± 0.8	16.5 ± 2.5
Pre-oxidized[b]	–	–	105 ± 10	6.7 ± 0.3[c]	13.5 ± 0.7	Nd
Pt[d]	–	–	155 ± 10	24 ± 1[c]	34.5 ± 1.5	Nd
Au[d]	–	–	165 ± 10	27 ± 1[c]	36.2 ± 1.5	32 ± 7
Ag[d]	–	–	None observed	None observed	37.0 ± 1.5	36 ± 8

[a] ZrNbO.
[b] Pre-oxidized ZrNbO.
[c] Pre-oxidized oxide thickness included.
[d] Pre-oxidized and coated ZrNbO.

imental values of m determined for ZrNbO in the chosen conditions are summarized in Table 2. Exponent values equal to 0.4 are greater than those reported for Zy-4 but it is worth emphasizing that this parameter strongly depends on material and oxidation environment [6–9].

The initial experimental results obtained on ZrNbO sheets coated with noble metals show increased oxidation rate compared to uncoated specimens (Fig. 2). Samples were pre-oxidized (oxide thickness of 1.1 ± 0.2 μm) at 500 °C in dry air before metal coating in order to avoid the potential formation of a ZrNbO–Pt intermetallic layer. As shown in Fig. 2, the pre-oxidation thermal treatment has no influence on the kinetic behaviour. Oxidation rate curve was obtained by the calculation of the experimental ratio $\Delta s/\Delta t$ (the difference between two successive oxide thicknesses measured divided by the oxidation time between those two measurements). Fig. 3 demonstrates that the oxidation rate is instantaneously higher by a factor of 3 when Pt is coated on ZrNbO. One can notice the initial oxidation rate increase for pre-oxidized ZrNbO. We have no interpretation on this fact. The higher oxidation rate for coated specimen clearly shows that the electrode material does not impede oxygen access to the ERS. The enhancement of the kinetics, which could be regarded as a 'catalytic' effect, is observed even for oxide thicknesses greater than 40 μm: At the end of the oxidation (300 h), the growth rate of Pt-coated ZrNbO is still 2.3 times greater than that obtained on uncoated specimen. As for the non pre-oxidized sample, a transition to a new sub-parabolic rate law is observed at 155 h (24 ± 3 μm) following a significant increase in the oxidation rate (Fig. 2).

In the case of gold coated ZrNbO, the kinetics is sub-parabolic, followed by an acceleration of the oxidation

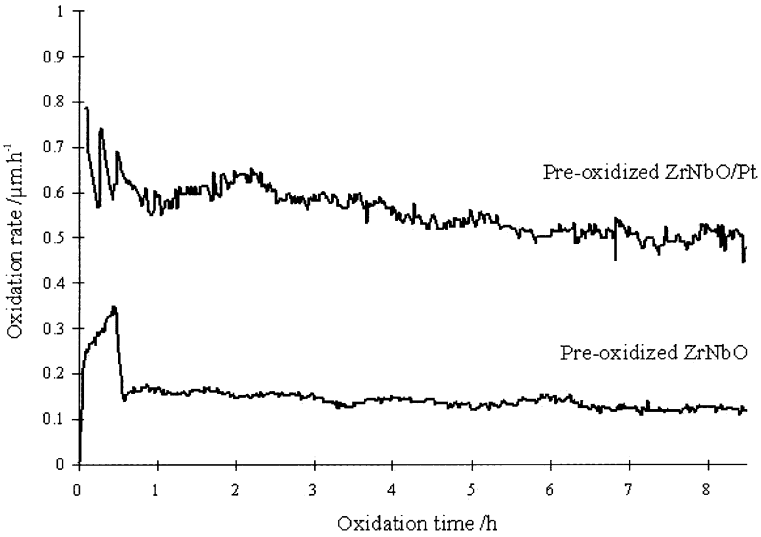

Fig. 3. Oxidation rate versus time determined by TGA for ZrNbO, pre-oxidized ZrNbO and pre-oxidized ZrNbO coated with Pt.

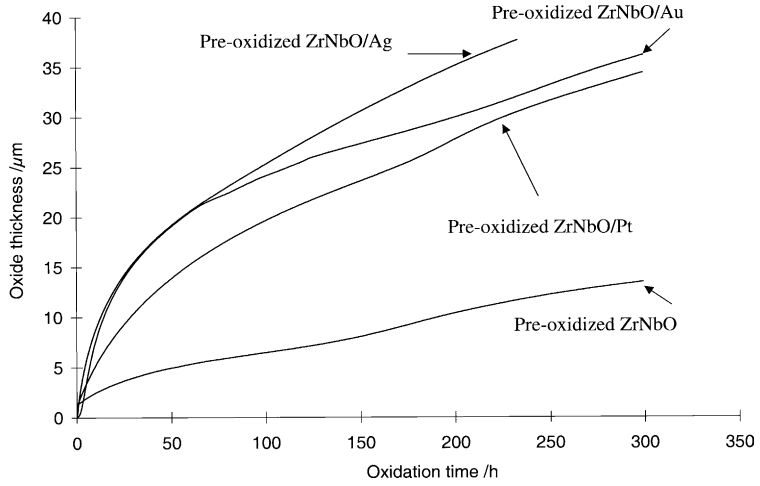

Fig. 4. Oxide thickness versus time determined by TGA for pre-oxidized ZrNbO, pre-oxidized ZrNbO coated with Pt, pre-oxidized ZrNbO coated with Au and pre-oxidized ZrNbO coated with Ag.

rate after 165 h (Fig. 4). Like the ZrNbO–Pt sample, the oxidation rate is higher than for uncoated specimen. The so-called catalytic effect was also detected after silver deposition but no kinetic transition was recorded during the oxidation experiment.

3.2. SEM examinations

For oxidation times longer than 100 h, SEM examinations show the presence of fine cracks on the surface of Pt-coated and uncoated ZrNbO (Fig. 5). After 120 h at 500 °C, the ZrO_2 surface (Fig. 6) is entirely covered with cracks for both types of sample. The occurrence of cracks does not depend on the pre-oxidizing treatment and these cracks are typically 1 μm wide (Fig. 7). The surface coverage of cracks represents 2% of the total area and the mean distance between the cracks was calculated to be around 110 μm, i.e., greater than the mean grain size of the investigated alloy (~5 μm). For times close to the kinetic transition, few cracks reach the metal/oxide interface and a localized enhancement of the oxide growth rate can be observed (Fig. 8). At the end of the experiment, the crack length does not go significantly beyond region of the kinetic transition. Fig. 9

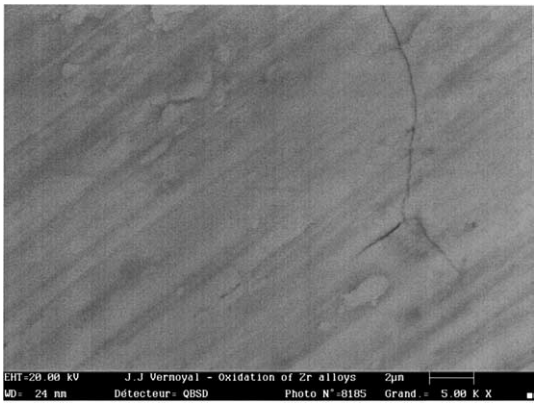

Fig. 5. Cross-section of the oxide film formed on uncoated ZrNbO sample. Specimen was exposed at 500 °C for 100 h.

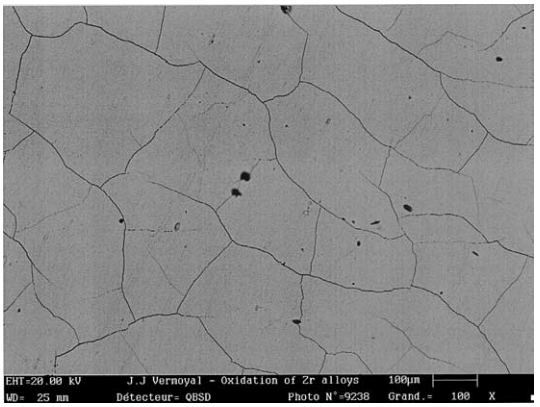

Fig. 6. External part of an oxide film formed on pre-oxidized ZrNbO/Pt sample. Specimen was exposed at 500 °C for 120 h.

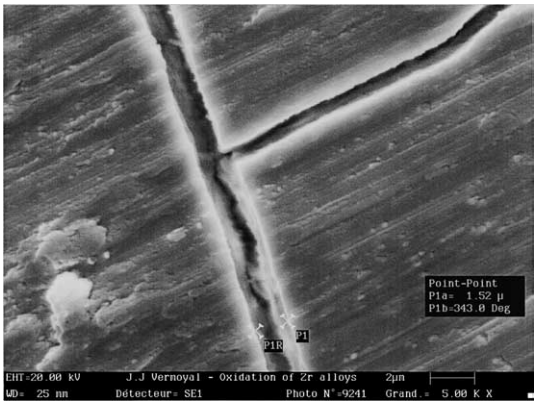

Fig. 7. External part of an oxide film formed on ZrNbO sample, detail of a crack. Specimen was exposed at 500 °C for 120 h.

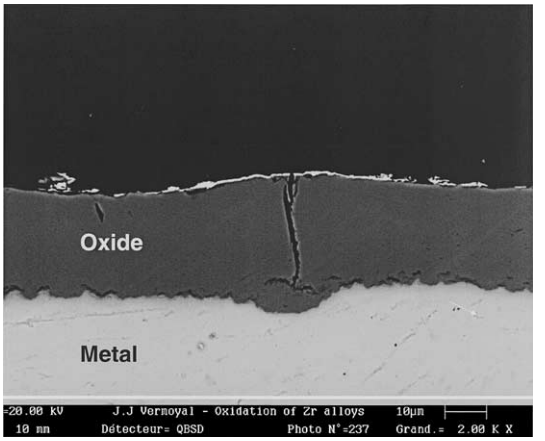

Fig. 8. Cross-section of an oxide film formed on pre-oxidized ZrNbO/Pt sample. Specimen was exposed at 500 °C for 160 h.

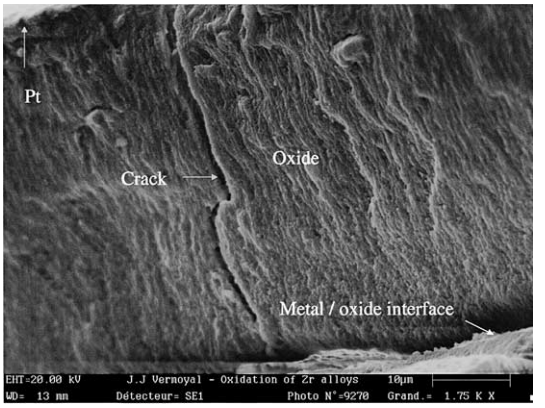

Fig. 9. Fracture cross-section of an oxide film formed on pre-oxidized ZrNbO/Pt sample. Specimen was exposed at 500 °C for 300 h.

shows that the oxide microstructure is mainly columnar. After 300 h at 500 °C, the oxide films formed on Au and Ag coated samples are similar to those observed with Pt deposits. Radial cracks do not reach the metal/oxide interface. It is worth noting that these radial cracks were not detected for ZrO_2 thicknesses up to 20 µm on Pt-coated Zy-4 [4].

Oxide thicknesses determined from SEM observations are in well agreement with those calculated from weight gains for all samples (coated and uncoated). Silver oxidation could be suspected at this temperature but it did not interfere in TGA measurements.

The other notable features of microscopic investigations can be summarized as follows:

- no metal diffusion proceeds within the oxide layer,
- no degradation of the Pt film occurs during the corrosion treatment,

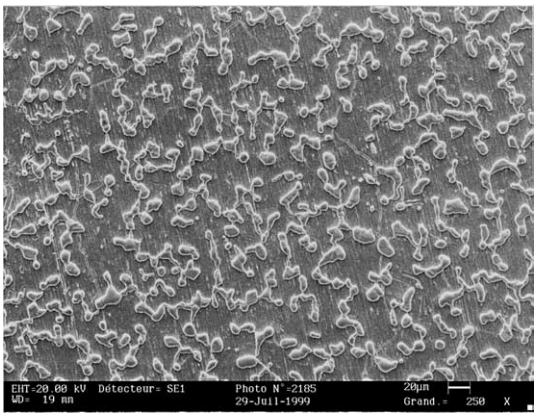

Fig. 10. External part of an oxide film formed on pre-oxidized ZrNbO/Ag sample. Specimen was exposed at 500 °C for 160 h.

- the morphology of both Au and Ag films is strongly altered in the chosen experimental conditions. After 160 h at 500 °C in dry air, a coalescence mechanism of gold and silver on the zirconia surface results in the formation of isolated and randomly interconnected silver or gold islands (Fig. 10). In order to check that this phenomenon does not depend on in situ experimental conditions, a silver wire was rolled around a ZrNbO tube before oxidation. After 160 h at 500 °C, Ag particles were observed on the tube surface, close to the silver wire. The mechanism (probably due to saturated vapour conditions of the noble metal) is outside the scope of this paper. Because of the modification of the electrode area during the oxidation, only one electrical experiment was performed with Au in order to obtain qualitative results.

3.3. Electrical characterizations

Electrical characterizations were performed on pre-oxidized ZrNbO in order to avoid any direct contact between the noble metals and zirconium alloy.

3.3.1. Cell potential

For oxidation times less than about 30 h, values of the potential difference E measured between Pt electrode and ZrNbO is a few millivolts (Fig. 11). However, a sharp peak is observed between 10 and 15 h. At longer oxidation times, E increases rapidly to 0.7–0.8 V and continues to increase up to 0.8–0.9 V independent of the noble metal.

3.3.2. EIS results at rest potential

For short oxidation periods (<30 h), the electrical response of ZrNbO/Pt is composed of two depressed overlapping semicircles in the Nyquist plane (Fig. 12). As expected for low impedance modulus at frequencies typically greater than 1 MHz, the inductive contribution of platinum wires and the resistance of the different elements composing the electrochemical cell are clearly observed on experimental diagrams. Only one single semicircle was described for an Au electrode. Beyond the stepwise increase of the potential difference E, three additional contributions to the high frequency (HF) semicircles were recorded (Fig. 13): a capacitive semicircle and an inductive contribution described in the low frequency (LF) range as well as another capacitive semicircle described in the medium frequency (MF) range which could only be resolved after subtraction of the two LF signatures. Inductive contribution has even been observed using Au electrode. In order to check the stability of the system at low frequencies, two successive

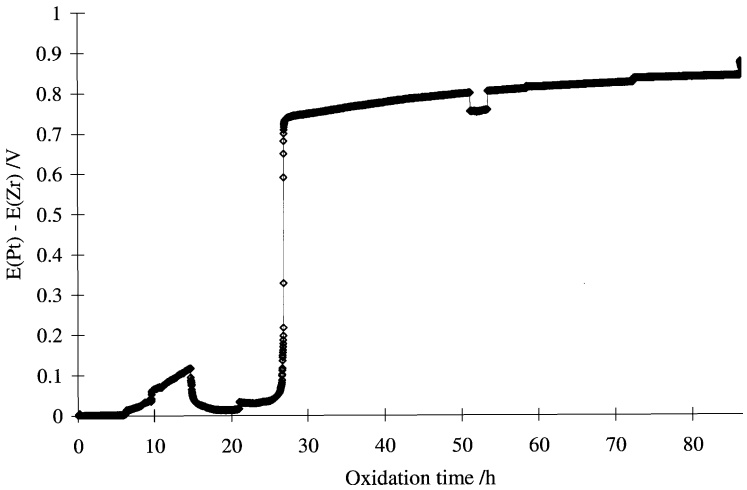

Fig. 11. Variation of the potential difference versus time for pre-oxidized ZrNbO/Pt.

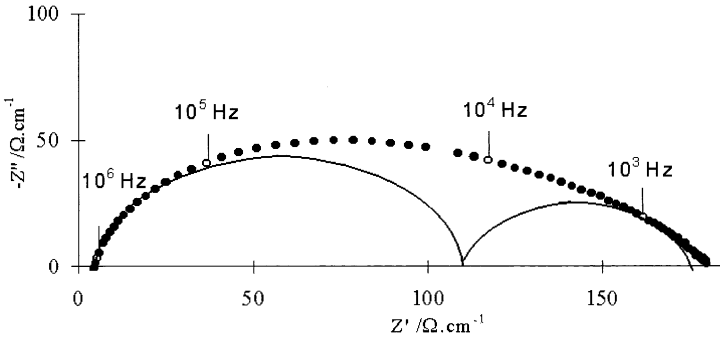

Fig. 12. Experimental Nyquist diagrams recorded in pre-transition period for pre-oxidized ZrNbO/pt after 30 h (o). Continuous line: schematic decomposition of the 2 signatures.

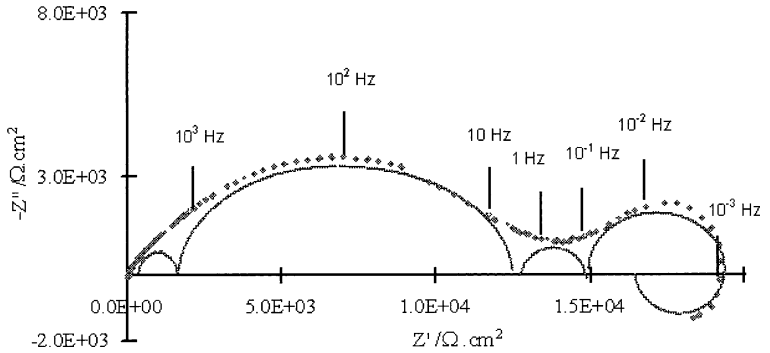

Fig. 13. Experimental Nyquist diagrams recorded after 50 h (o) for pre-oxidized ZrNbO/Pt. Continuous line: schematic decomposition of the 5 signatures (see text for further explanations).

impedance diagrams were obtained by decreasing and increasing the ac measuring frequency. The superposition of both diagrams indicates the validity of EIS measurements without no modification of the corrosion process (due to bias imposed during the EIS measurements).

HF impedance modulus for ZrNbO/Pt increase as a function of oxidation time whereas the magnitudes of the LF contributions are not significantly modified. No variation in the impedance diagram shape and in the modulus has been observed for oxidation times close to the kinetic transition. Since the gold electrode area is a decreasing function of time (as described above), no normalized impedance diagrams could be presented. Thus, the time modifications of EIS characterization for this system could only be regarded as qualitative because of the difficulties of separating the relevant effects of the metal electrode, the oxide growth contributions and possible interfacial mechanism. Nevertheless, ZrNbO/Au could give complementary information on short range time studies, as for instance the study of the influence of polarization on impedance diagram shapes during the corrosion process.

3.3.3. Polarization curves

It is difficult to determine the potential distribution at both interfaces when a dc bias is applied on an asymmetrical cell. By defining the bias in reference to the oxygen reduction at the outer surface one can expect that

(i) under cathodic polarization (i.e. $E < E_{\text{corrosion}}$), oxygen reduction at the ZrO_2/electrode interface and oxidation of zirconium at the inner interface might be enhanced;
(ii) under anodic polarizations (i.e. $E > E_{\text{corrosion}}$), zirconia might be reduced at the metal/oxide interface while the oxide ions might be oxidized at the ZrO_2/electrode interface. As electrons are the main charge carriers in oxide formed on ZrNbO [10], the ZrO_2 reduction is unlikely to be predominant.

Linear sweep voltametry was carried out to observe general shape and check that total resistances measured on impedance diagrams are equal to the reciprocal slopes of the I–(E) curves. Voltamograms were recorded after 53, 97 and 177 h for ZrNbO/Pt (Fig. 14)

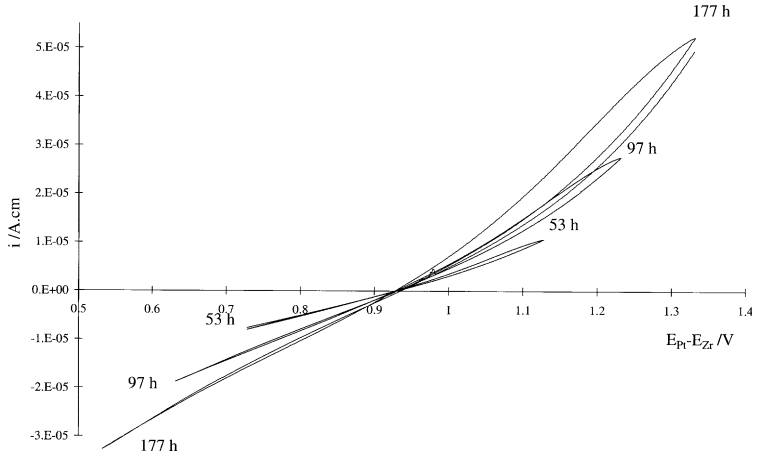

Fig. 14. Linear voltamogram curves recorded after 53, 97 and 177 h for pre-oxidized ZrNbO/Pt.

and 180 h for ZrNbO/Au, respectively. Anodic curves obtained on ZrNbO/Pt exhibit a hysteresis which is an increasing function of the scan rate but which do not depend on the oxide growth since forward and backward scans are identical. Let us mention that no linear variation was detected for high bias values on Tafel plots.

3.3.4. Influence of the cell polarization on impedance diagrams

For polarization study, LF were limited to 10^{-3} Hz in order to avoid any interference with both the oxide growth and electrical change due to bias. The time for pre-polarization (before EIS measurements) was 10 min. This time was chosen to be sure that electrical equilibrium was reached in the oxide film. Regardless of the electrode material, the application of a cathodic or anodic bias to the electrochemical cell decreases the magnitudes of the LF contributions while the HF one remains unchanged for $t < 70$ h. After each polarization test, impedance diagrams were obtained at an initial corrosion potential so that any bias applied would not modify the electrochemical response of the system. For oxidation time greater than 80 h, this part of impedance diagrams is slightly changed under polarization (Fig. 15). We respectively observed both a small decrease in the impedance modulus for anodic polarization (4% at 0.5 V (80 h) as compared to the value measured at the corrosion potential $E = 0.9$ V) and a weak increase under cathodic bias (close to 3% at 1.1 V as compared to the value obtained at the corrosion potential). The presence of the inductive signature in the case of the higher cathodic bias (1.2 V) was observed in Fig. 15 just for one curve.

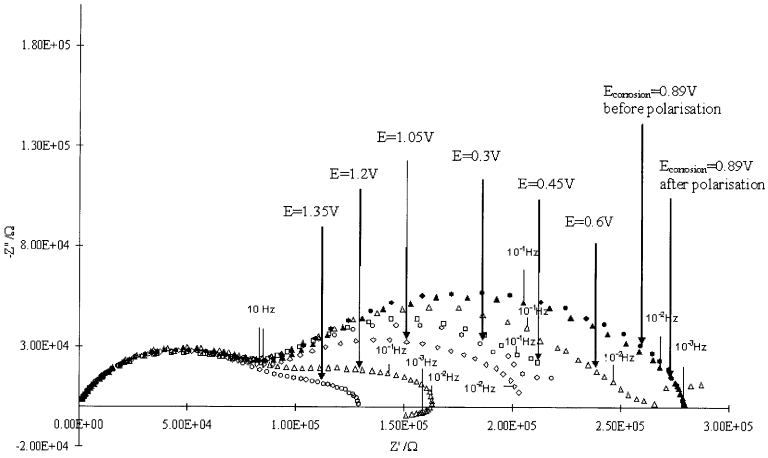

Fig. 15. Experimental Nyquist diagrams recorded after 70 h for pre-oxidized ZrNbO/Au at different bias ($E = E_{Au} - E_{Zr}$).

4. Discussion

4.1. Oxidation kinetics

In the case of Zy-4, thermogravimetric studies have shown that the oxidation kinetic are not modified for platinum coated sheets [4]. By correlating with in situ EIS investigations, the corresponding oxidation behaviour was thus proposed to be consistent with a process in which oxygen diffusion is the rate-determining step. In the current study, the presence of noble metals, well known to catalyze oxygen reduction (see below), gives rise to an enhancement of the oxide growth on ZrNbO. The fact that oxidation rate increases when noble metal are coated on ZrNbO clearly demonstrates the permeability of the metal layer (the porosity of noble metal was not characterized). Therefore, oxygen diffusion cannot be regarded as the pure rate determining step. Accelerated corrosion has also been observed at 700 °C after deposition of gold on pure Van Arkel Zr foils even with pre-oxidized films [11]. Gold is notorious for diffusing into zirconia films at high temperatures and is thought to potentially affect the kinetics by modifying the oxide crystallites growth. Nevertheless, results obtained with other noble metals must be considered in order to explain the kinetic acceleration of oxidation for coated specimens. In this way, the catalytic effect due to Pt or Ag film (10–30 nm thickness) coated on pure Zr was reported by Fiegna and Weisberger [12] in water vapour at 450 °C, and with Pt coupling in oxygen. The instantaneous kinetic acceleration for pre-oxidized film and the steady higher oxidation rate recorded for zirconia films thicker than 30 μm cannot be explained either by modification of the ZrO_2 properties (microstructure, cracks, diffusion of the noble metal, etc.) or by a high electrical field mechanism on film growth.

From an electrochemical point of view, noble metal coating of the oxide surface is likely to modify the oxidation rate of zirconium alloys if the determining step involves an interfacial process such as oxygen reduction. By comparing kinetic curves, Frichet et al. [13] proposed that the rate-determining step during the pre-transition stage is oxygen diffusion for Zy-4 and a multi-steps process (interfacial reaction-oxygen diffusion) for ZrNbO under a low oxygen pressure environment (100 mbars, 470 °C). The current TGA experiments demonstrate that ZrNbO oxidation is at least partially controlled by the oxygen reduction process. In a previous paper [10], we observed that the increase in thickness of a dense oxide layer formed on ZrNbO at 360 °C in water (and studied ex situ by EIS) was related to a constant oxidation rate. Such behaviour suggests that the rate controlling process is not a pure oxygen diffusion mechanism through ZrO_2 as generally assumed. Further study is needed to check if the corrosion mechanism proposed for ZrNbO gaseous oxidation can be applied to a high temperature water environment.

This is quite surprising to note a higher oxidation rate for Au coated specimen despite the fact that the catalytic effect on oxidation reduction is known to be higher for Pt than Au. Even in the case of an additional contribution due to Pt grid when Au coating became very small, the oxidation rate should not be higher because

(i) of the grid nature, it is the same electrode material as for ZrNbO/Pt so oxidation rate should not be higher
(ii) Pt grid is a non-porous material so the contact area for oxygen reduction (three-phase boundary, see Section 4.4 for details) is several orders of magnitude lower that in the case of PVD deposit.

Breiter et al. [14,15] investigated electrochemical processes occurring at the interface of gold and Pt/Yttria-stabilized zirconia by cyclic voltametry and potentiostatic current–potential curves. They noticed that the polarization resistance are larger by nearly one order of magnitude for Au/YSZ than those for Pt/YSZ. Contrary to Pt electrodes, it seems that the electrochemical formation and reduction of an oxide are reflected by the shape of cyclic voltamograms. Nevertheless, more work is required to understand the high oxidation rate in the present case for Au and Pt coating compared to the rate of charge transfer for ceramic/electrode systems.

4.2. Kinetic transition

As for the Zy-4 kinetic transition, for which a large number of localized degradations of the oxidation resistance would lead to a global acceleration of the kinetics [2,4], the modification of the oxidation curve observed after 150 h for uncoated and Pt- or Au-coated ZrNbO (Figs. 2 and 4) would result from a mechanical rupture of the oxide film. While only circumferential cracks can be observed on oxide film formed on Zy-4 [4], SEM examinations suggest that the acceleration of the oxidation rate for ZrNbO would be correlated to the growth of radials cracks down to the metal oxide interface (Fig. 9). Localized accelerated corrosion depicted at the crack tips (Fig. 8) undoubtedly indicate that the fracture of the oxide film does not arise from thermal stress changes during cooling but rather results from the intrinsic dynamic mechanism of the oxidation process. In the case of ZrNbO/Ag, no cracks were detected that reached the inner interface on the different samples investigated. Considering that the oxidation rate was the highest for this noble metal (Fig. 4), a competition between ZrO_2 growth and crack propagation through the oxide layer can be assumed. In the case of Pt coating, the kinetics transition occurs beyond 155 h and at an oxide thickness less than that for ZrNbO/Au.

In the case of ZrNbO/Ag, the crack propagation rate may be too slow to be detected and has not reached the metal/oxide interface to give rise to the kinetics transition.

4.3. Electrical characterizations

4.3.1. Cell potential

As previously detailed for Zy-4 oxidation in the same oxidative conditions [4], the appearance of a low potential difference during the first hours of oxidation treatment has been related to the high level of non-stoichiometry of the oxide and a main electronic contribution. The occurrence of short-circuits sometimes reported in the literature for Zy-4 [16,17] was not detected for ZrNbO. Short-circuits are often proposed to result from the local conduction of intermetallic particles (mainly β-Nb with a mean diameter close to 50 nm and few $Zr(Nb,Fe,Cr)_2$ smaller than 300 nm for ZrNbO). At this stage, the origin of the sudden potential step in the coated condition (Fig. 11) is still unclear. Even if this observation could be linked to any variation of the oxide electronic properties, no significant modification of the corrosion kinetics was detected during this time.

4.3.2. In situ electrochemical characterizations

The interpretation of impedance diagrams in situ recorded during corrosion of zirconium alloys in high temperature water or by ex situ characterization in liquid medium at room temperature [4,5,17–22] is still controversial. Electrical contributions are sometimes associated with the oxide response only [18,20,22] or the Faradaic process [23]. The best way to identify electrical responses is to modify experimental parameters for example the electrolyte composition [18], the ion concentrations [22] or the temperature [4,6]. Even in these cases, the analysis in terms of equivalent circuits is not straightforward. The results of our previous EIS measurements in a gaseous atmosphere [4,5,10] emphasize the need to use the Jonscher universal law for the dielectric response of the oxide film. This complex capacitance is defined as the sum of a pure capacitance C_∞, associated with the oxide thickness, and a dispersion contribution commonly used to characterize the dielectric properties, the constant phase element (CPE). As often quoted in the literature, it is worth noting that this latter parameter has no unequivocal physical interpretation. As experimental impedance diagrams are composed of several signatures, we propose to estimate the order of magnitude and time evolution in order to try to identify EIS signatures recorded on ZrNbO/Pt. Data were analyzed using the following series connection R_c–($R_1C_{\text{Jonscher-1}}$)–($R_2C_{\text{Jonscher-2}}$)–($R_3\text{CPE}_3$)–(R_4C_4)–($R_5C_{\text{inductive}}$), where R_c represents the overall resistance of contacts and connection wires, $R_1C_{\text{Jonscher-1}}$ and $R_2C_{\text{Jonscher-2}}$ are associated with HF contribution, $R_3\text{CPE}_3$ is related to the MF depressed semicircle, R_4C_4 and $R_3C_{\text{inductive}}$ are used to estimate characteristic values of the two LF contributions.

Capacitance: During in situ investigations on Zy-4 [4] in the same oxidation states, the two described impedance contributions were assigned to a porous and a dense ZrO_2 layers. Referring to the literature on the zirconium alloys oxidation [2], the oxide film would degrade to a partially porous one during the post-transition step. The value of the capacitance C_∞ extrapolated at infinite frequency on Cole–Cole diagrams is related to the total thickness considering a permittivity ε equal to 24 at 500 °C. For ZrNbO/Pt at 500 °C, $C_{\text{Jonscher-1}}$ and $C_{\text{Jonscher-2}}$ are of the order of nF cm^{-2} in good agreement with typical oxide responses (Fig. 16). The $C_{\text{Jonscher-1}}$ values are nearly identical to those of C_∞. Assuming that ε is close to 20 at room temperature for

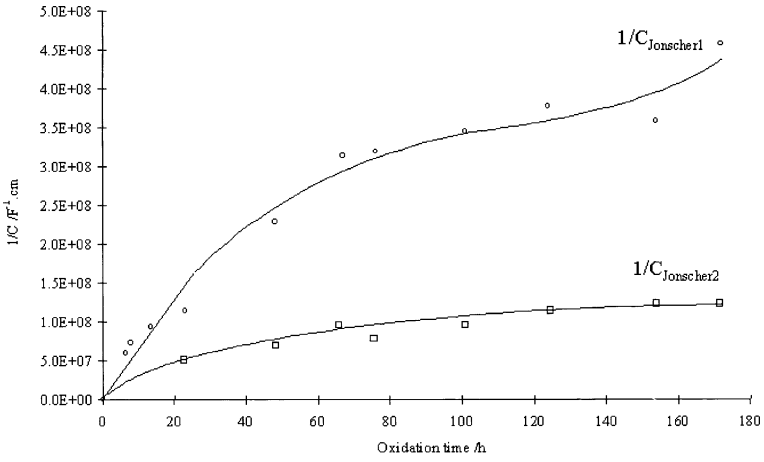

Fig. 16. Variation of the reciprocal of $C_{\text{Jonscher-1}}$ and $C_{\text{Jonscher-2}}$ versus oxidation time for pre-oxidized ZrNbO/Pt.

zirconium dioxide formed on ZrNbO [10], and according to the procedure proposed in [4] to estimate the permittivity at 500 °C, a reproducible value of 75 was thus calculated. A factor close to 4 between ε at 25 and 500 °C (20 and 75 respectively) cannot be simply associated with the activation of dielectric properties of the oxide. As previously shown [5,10], the intrinsic capacitance of the oxide film is not readily accessible for frequencies typically lower than 1 MHz at 500 °C. However, the time evolution of reciprocal $C_{\text{Jonscher-1}}$ follows the shape of the kinetics curve of ZrNbO/Pt (Fig. 16), strongly suggesting a correlation between this HF contribution and the oxide film growth during the pre-transition stage. The variation of reciprocal $C_{\text{Jonscher-2}}$ obeys a parabolic law as a function of oxidation time (Fig. 16). Values for CPE_3 and C_4 are roughly equal to a few mF cm^{-2} and $C_{\text{inductive}}$ values are close to 0.2 and 0.3 F cm^{-2}.

Resistance: For low values of potential difference E (i.e. oxidation times less than 40 h), the variation of both HF resistances do not obey either a simple law (parabolic for instance) or a law similar to the oxidation kinetics (Fig. 17). Beyond the stepwise potential jump of the potential difference (i.e. $t > 40$ h), R_1 and R_2 are also increasing functions of oxidation time. As mentioned previously [4], the time constant RC can be regarded as the resistivity of an oxide layer by assuming a constant permittivity during the oxide growth. For both HF contributions, this product does not depend on oxidation time and the corresponding resistivities are respectively equal to 1 KΩ cm and 0.7 MΩ cm for signatures 1 and 2. If these two contributions are related to the bulk of the oxide, this suggests a simple geometric growth of zirconia. R_3 remains relatively unchanged close to 5 KΩ cm^{-2} between 80 and 180 h whereas a two-fold increase of R_4 was recorded (Fig. 18). The resistance

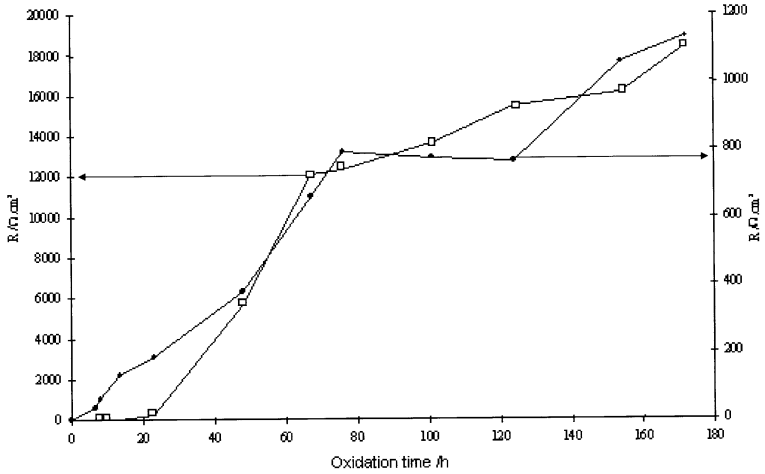

Fig. 17. Variation of the resistance (●) R_1, and (□) R_2 versus oxidation time for pre-oxidized ZrNbO/Pt.

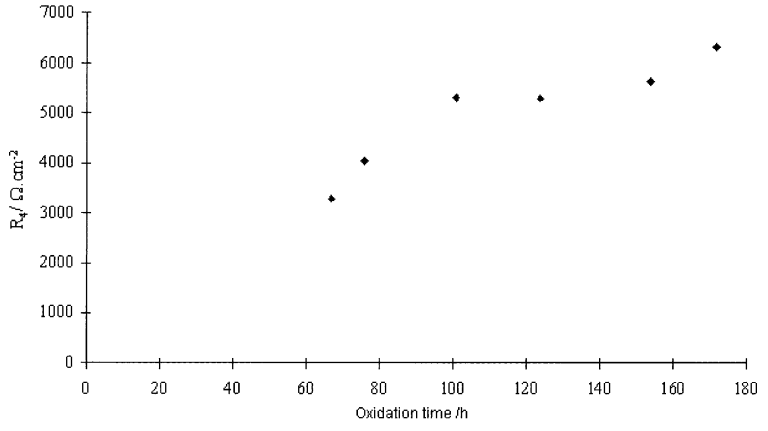

Fig. 18. Variation of the resistance R_4 versus oxidation time for pre-oxidized ZrNbO/Pt.

associated with the inductive loop cannot be monitored accurately due to the low experimental resolution, but a value close to 3 $K\Omega cm^{-2}$ is estimated for the whole oxidation treatment.

Dispersion index: As for related resistivities, dispersion indexes associated to dielectric dispersion of signatures 1 and 2 remain unchanged around 0.6 and 0.7, respectively.

Regardless of the catalytic effect of the noble metals on oxidation kinetics, the impedance shape of LF responses, the order of magnitude of corresponding capacitive contributions and, above all, the influence of polarization clearly indicate the implication of at least one interfacial process in the oxidation mechanism of ZrNbO/M (M = Pt or Au). The significant decrease of impedance modulus under bias is typical of what is generally observed for electrochemical and interfacial processes. The evidence of an inductive signature is often believed due to adsorbed intermediate species [24] in the case of oxygen reduction on solid electrolytes. For instance, Van Hassel et al. [25] showed that such a contribution depends on rate constants of the different elementary steps of the reaction process and on the surface coverage of adsorbed species. Capacitance values about a few millifarads have been defined by some authors as 'pseudo-capacitances' related to the presence of oxygen close to the oxide/electrode interface. 'Pseudo' means that the chemical nature of this capacitance is quite different from the classical electrical double layer [26]. Capacitances of 0.7 $mF cm^{-2}$ have been interpreted in terms of electron injection at the oxide/electrode interface not compensated by oxygen transport [27]. Concerning the order of magnitude ($F cm^{-2}$ in this work compared to $mF cm^{-2}$), we have to bear in mind that the present system is quite different from solid electrolyte coated with noble metal. Electrons engaged in the reaction reduction are provided by the oxidation of Zr at the metal oxide interface and not only from the electrode material as in the latter case. This can significantly changes the order of magnitude of electrical components associated to the electrochemical system. The literature is very poor in such a field.

As a complement to LF interfacial signatures, the independence of the HF part of the impedance diagrams under polarization for short oxidation time (Fig. 12) could indicate the bi-layered structure of the oxide film (i.e. a dense and a porous part) [4,5,22]. The dense and porous part of the oxide deduced from EIS measurements may probably depend of very fine porosity not detected from microscopic examinations (only micrometric cracks can be distinguished from SEM observations in Fig. 8). Nevertheless, it could be interesting to performed EIS measurements in liquid medium where the electrolyte soaked the pores of the oxide films in order to compare to the results of the present paper (see for instance Ref. [10]).

The increase of HF impedance modulus can be regarded as resulting from the geometrical growth of each part of zirconia since electrical properties (dispersion index and resistivity) remain unchanged during the whole corrosion treatment. The oxide thickness on ZrNbO/Pt cannot be directly determined from C_∞ extrapolation although the modification of this parameter is related to the oxide growth. The origin of the HF signature referenced as ($R_2C_{\text{Jonscher-2}}$) for Pt coated alloy must be cautiously interpreted since no evidence could be deduced over the time period of experiment. Nevertheless, remembering that oxide ions are the only charge carriers engaged into the process of oxide formation, it is not unreasonable to connect this contribution to a part of the oxide. The application of a bias could enhance the oxygen reduction rate and thus increase the oxide ions concentration in the zirconia matrix, at least in the vicinity of the outer interface, and consistent with a decrease in the overall zirconia conductivity. Higher is the concentration of oxide ions in zirconia, lower is the concentration of vacancies, and then, lower is the overall zirconia conductivity. In favour of this assumption, non-uniform distributions of oxygen vacancies have been clearly observed in yttria-doped tetragonal zirconia under electric fields [28–30]. This effect may be relevant when sufficiently high oxide thicknesses result in oxygen diffusion becoming partially limiting.

At this stage, let us mention that the observed differences between EIS signatures recorded for Pt and Au electrodes cannot readily be interpreted in terms of electrical properties of the oxide film or interfacial mechanisms (see below). More work is needed in order to gain a better insight, but present results support the assumption of a change in oxidation resistance as a function of the nature of the noble metal as established from oxidation kinetics.

4.4. Oxidation mechanism-rate determining step

The two experimental approaches adopted in this study indicate that at least one step of the oxygen reduction mechanism partially controls the oxidation rate of ZrNbO. The fact that the oxidation curve of this alloy is not linear shows that reduction is not the only process which governs the oxide growth (except if the rate of the electrochemical process decreases which is fairly unlikely as explained below). Moreover, the presence of noble metal coating on ZrNbO is not sufficient to enhance the interfacial process rate until the coating influence disappears since related interfacial signatures can be observed on EIS diagrams. In this part of the paper, we discuss the electrochemical step that may be involved in the oxidation process and try to identify the nature of the rate-determining oxidation steps.

In terms of electrode process on a solid electrolyte, an electrochemical reaction is typically regarded as a charge-transfer process occurring across a two-dimensional interface between phases. Many workers have proposed this concept by treating the three-phase boundary TPB (gas-electrode-electrolyte) as a one-dimensional 'interface' where the reaction is confined [31,32]. The oxygen reduction proceeds where there is a simultaneous presence of oxygen vacancies, electrons and gaseous oxygen. This reaction has been extensively studied in the understanding of cathodic polarizations in the solid oxide fuel cells (SOFC) [33,34]. In this case, the electrons involved in the reduction process necessarily come from the noble metal (Pt, Ag, Au) used as the electrode material. Despite the numerous studies on this topic, there is no consensus on the identification of the rate determining step which appears to depend on the nature of the electrode, its morphology (porosity, surface coverage) [35] and more generally, by the experimental conditions (temperature, oxygen partial pressure, etc.). For Pt on zirconia, different reaction models have been developed according to the following processes:

- oxygen diffusion in pores,
- oxygen adsorption on the electrode and/or electrolyte,
- dissociation of oxygen molecules into atoms,
- oxygen atoms diffusion in the electrode,
- electrons diffusion in the electrolyte,
- oxide ions diffusion in the electrolyte (zirconia),
- charge transfer reaction.

In the case of a mixed conductor (exhibiting ionic and electronic conductions), and so, for the oxide film formed on ZrNbO, the oxygen reaction mechanism involves multiple steps occurring at different locations in a macroscopically defined three-dimensional space. Charge transfer localization can be quite different when compared to the same process taking place on a pure ionic conductor. Accordingly, the relative complexity of experimental EIS diagrams cannot directly lead to modelling of the electrochemical response. Obviously, further investigations based on the influence of oxygen partial pressure, temperature and electrode area on the EIS characterizations are needed. Nevertheless, the noble metals used in the current study influence quite differently the oxygen reduction. The relationships between these influences and the oxidation kinetics can be discussed to get a better understanding of the oxidation mechanism of ZrNbO in dry air.

Platinum is well known to catalyze oxygen reduction on solid electrolytes. O_2 easily adsorbs on Pt with a small activation energy around 12 kJ mol^{-1} [36]. Thermal dissociation of adsorbed oxygen is characterized by a high enthalpy close to 220–290 kJ mol^{-1} [37]. Atomic oxygen diffusion at the electrode surface then proceeds with an activation energy of the order of 140 kJ mol^{-1}. The oxygen reduction mainly occurs at the TPB (Pt-zirconia-gas) since platinum does not significantly dissolve oxygen species in its volume at this temperature. According to Van Dijk et al. [27], oxygen reduction on ionic and mixed conductors coated with Pt would be controlled by a diffusion process from adsorption sites towards the ERS, probably located on the oxide surface.

In the case of a gold electrode, the kinetic reaction also takes place at the TPB but the reduction kinetics are weakly lower than with platinum. Oxygen chemisorption on gold is only significant at high temperatures and is greatly influenced by impurities (Ca or Si) at the noble metal surface [38]. Whatever the situation, adsorption would induce the formation of a complex strongly bonded to the surface. A few adsorbed species could migrate from the electrode surface down to the ERS. Regarding the silver deposit, oxygen is greatly dissolved in the electrode so the ERS for O_2 reduction are extended to the whole Ag/ZrO_2 contact area.

Noting that the oxidation rate is slightly higher for Au coating compared to Pt (Fig. 4), the different kinetics may not result from the adsorption properties of the electrode. The adsorption step suggested by impedance measurements is probably the adsorption of oxygen on zirconia. If this process, the adsorption of oxygen on zirconia, is the unique limiting factor, then the nature of the noble metal would not be expected to have a significant influence on oxidation kinetics. Since Pt, Ag and Au exhibit different catalytic properties, it is concluded that another electrochemical process is involved at the TPB. As no diffusion impedance is observed during EIS investigations, oxygen diffusion through the oxide layer, if any, is not the only limiting process and charge transfer is likely to be a second determining step of the oxidation. The assumption of adsorption and charge transfer involved in the oxidation of coated specimens can be extended for uncoated ZrNbO since electrochemical kinetics are lower without the noble metal (noble metal just enhances the rate of the rate-determining steps). As mentioned above, the non-linear oxidation rate for both coated and uncoated samples can be explained either by modifying the nature of the rate-determining step (a transition from an interfacial to a diffusion control) or by a decreasing interfacial process rate (loss of catalytic impact because of cracks surface enhancement, etc.). Since the decrease of oxidation rate is effective for coated and uncoated specimens, the decrease of interfacial process rate is most unlikely. It is not possible to deduce differences between Au and Ag because of modifications of the electrode contact area during oxidation.

Accordingly, and by taking into account the former case (interfacial to diffusion control), the nature of the rate determining step for ZrNbO oxidation at 500 °C in air might be a mixed kinetics process of

adsorption-charge transfer-diffusion. This kind of situation, where both electrochemical reaction and diffusion contribute to the kinetics limitation, was treated early in the case of steels [39–41] and was popularized by Deal and Grove [42] for the oxidation of silicon. Up to now, the thermal oxidation of metals has been described in terms of diffusion limited kinetics, where a continuous decrease of the diffusion coefficient of predominant defects through the oxide is responsible for the deviation from the parabolic rate law. Deal and Grove [42] have shown that stationary mixed kinetics, where both reaction and diffusion of charge point defects are limiting processes, also lead to a sub-parabolic rate law, although the diffusion coefficient remains constant with time.

In the present case, a higher oxidation rate for noble metal coated samples as compared to uncoated samples and complex EIS signatures (without evidence of any impedance diffusion), identified as electrochemical processes, was observed for high oxide thicknesses (30 μm). This means that the kinetics are still mainly controlled by an interfacial process during the duration of experiments and that oxygen reduction still partially controls the oxidation rate even when noble metals are present on ZrNbO (no EIS signature would be observed if the electrochemical step were not controlling the oxidation rate, see Ref. [4] and the case of Zy-4 for example). A kinetic model based on this assumption will be presented in a future paper.

Under PWR operating conditions, the corrosion resistance is known to be significantly higher for ZrNbO than for Zy-4 [43]. The microstructure of the oxides formed on Zy-4 and ZrNbO are degraded (roughness of the metal/oxide interface, distribution of radial cracks) [44], but only the Zy-4 corrosion rate drastically increases. The conclusion of the present paper dealing with the interfacial controlling process for ZrNbO could explain why the degradation of the oxide microstructure is not as detrimental for this alloy as compared for Zy-4. In the latter case, reduction of the protective (dense) oxide thickness increases the oxygen flux and so the corrosion rate (considering the assumption of a pure oxidizing species diffusion mechanism). For ZrNbO, interfacial reactions are not or weakly modified by any variation in the ZrO_2 microstructure and thus the corrosion resistance remains unchanged during exposure in reactor.

5. Conclusion

The oxidation of ZrNb(l%)O(0.13%) covered with different noble metal (Pt, Au, Ag) was investigated in situ at 500 °C in dry air by thermogravimetric analysis and electrochemical impedance spectroscopy. Noble metals were observed to clearly modify the oxidation rate, even if a pre-oxidized zirconia film was formed before deposit. The enhancement in oxidation rate is always greater for large oxide thicknesses (30 μm). Localized oxidation rate increase for oxide thicknesses around 10 μm and oxidation times close to 100 h were proposed to explain the kinetic transition. Catalytic effects observed when noble metal are coated on ZrNb(l%)O(0.13%) suggest that the mechanism controlling oxidation is not a pure oxygen diffusion process through the oxide layer. The increase in the oxygen reduction reaction at the oxide/metal/gas interface partially controls the oxidation kinetics of ZrNb(l%)O(0.13%). Complex electrical signatures monitored during the oxide growth corroborate this assumption and hence indicate that the oxygen reduction still partially controls the oxidation rate when noble metal are present on the ZrNb(l%)O(0.13%) surface. Finally, a mixed process of interfacial-diffusion mechanism is proposed to be the rate determining step for ZrNb(l%)O(0.13%) oxidation in dry air.

References

[1] B. Cox, J.P. Pemsler, J. Nucl. Mater. 28 (1968) 73.
[2] Waterside Corrosion of Zirconium Alloys in Nuclear Power Plants, IAEA-TECDOC-996, IAEA, Vienna, 1998.
[3] A. Grandjean, Y. Serruys, J. Nucl. Mater. 273 (1999) 11.
[4] J.J. Vermoyal, L. Dessemond, A. Hammou, A. Frichet, J. Nucl. Mater. 298 (2001) 297.
[5] J.J. Vermoyal, A. Frichet, L. Dessemond, A. Hammou, Electrochim. Acta 45 (1999) 1039.
[6] C.M. Eucken, in: Proceedings of the Eighth Symposium of the Zirconium in the Nuclear Industry, ASTM-STP 1023, American Society for Testing and Materials, Philadelphia, 1989, p. 113.
[7] P. Kofstad, Acta Chem. Scand. 12 (1958) 701.
[8] E.A. Gulbransen, K.F. Andrew, J. Metals 9 (1957) 394.
[9] J. Belle, M.W. Mallett, J. Electrochem. Soc. 101 (1954) 339.
[10] J.J. Vermoyal, A. Frichet, L. Dessemond, A. Hammou, Electrochim. Acta 47 (2002) 2679.
[11] D. Bradhurst, J. Draley, J. Van Drunen, J. Electrochem. Soc. 112 (1965) 1171.
[12] A. Fiegna, P. Weisberger, J. Electrochem. Soc. 115 (1968) 369.
[13] A. Frichet, P. Barberis, N. Petigny, in: 12th Symposium on Zirconium the Nuclear Industry, Toronto, Poster Session, 15–18 June 1998.
[14] M. Breiter, K. Leeb, G. Falfilek, J. Electroanalyt. Soc. 434 (1997) 129.
[15] M. Breiter, K. Leeb, G. Falfilek, J. Electroanalyt. Soc. 436 (1997) 155.
[16] O. Gebhardt, J. Nucl. Mater. 203 (1993) 17.
[17] B. Cox, Y.M. Wong, J. Nucl. Mater. 218 (1995) 324.
[18] C. Bataillon, S. Brunet, Electrochim. Acta 39 (1994) 455.
[19] B. Cox, F. Gascoin, Y.M. Wong, J. Nucl. Mater. 218 (1995) 113.
[20] J. Schefold, D. Lincot, J.C. Badot, O. Kerrec, in: Proceedings of the Symposium on Passivity and its

Breakdown, Electrochem. Soc., Pennington, USA, 1998, p. 740.
[21] G. Nagy, Z. Kerner, T. Pajkossy, J. Nucl. Mater. 300 (2002) 230.
[22] P. Barberis, A. Frichet, J. Nucl. Mater. 273 (1999) 182.
[23] H. Göhr, J. Schaller, H. Ruhman, F. Garzarolli, in: Proceedings of the 11th Symposium of the Zirconium in the Nuclear Industry, ASTM-STP 1295, American Society for Testing and Materials, 1996, p. 181.
[24] R.D. Armstrong, M. Henderson, J. Electroanal. Chem. 39 (1972) 81.
[25] B.A. Van Hassel, B.A. Boukamp, A.J. Burggraaf, Solid State Ionics 48 (1991) 155.
[26] M. Kleitz, Solid State Ionics 314 (1981) 513.
[27] M.P. Van Dijk, K.J. De Vries, A.J. Burggraaf, Solid State Ionics 21 (1986) 83.
[28] S.P.S. Badwal, N. Nardella, Appl. Phys. A 49 (1989) 13.
[29] X. Lu, K. Liang, S. Gu, Y. Zhong, H. Fang, J. Mater. Sci. 32 (1997) 6653.
[30] D.-J. Kim, H.-J. Jung, J.-W. Jang, H.-L. Lee, J. Am. Ceram. Soc. 81 (1998) 2309.
[31] N. Robertson, J. Michaels, J. Electrochem. Soc. 137 (1990) 129.
[32] N. Robertson, J. Michaels, J. Electrochem. Soc. 138 (1991) 1494.
[33] E. Siebert, Electrochim. Acta 39 (1994) 1621.
[34] B.C.H. Steele, Solid State Ionics 86–88 (1996) 1223.
[35] M.J. Verkerk, M.W. Hammink, A.J. Burggraaf, J. Electrochem. Soc. 130 (1983) 71.
[36] C.W. Tucker, J. Appl. Phys. 35 (1964) 1897.
[37] T. Gür, I. Raistrick, R. Huggins, J. Electrochem. Soc. 12 (1980) 2620.
[38] B. Nguyen, L.M. Rincon-Rubio, D.M. Mason, J. Electrochem. Soc. 9 (1986) 1860.
[39] U.R. Evans, Trans. Electrochem. Soc. 46 (1924) 247.
[40] K. Fischbeck, Z. Elektrochem. 39 (1993) 316.
[41] H. Nöldge, Phys. Z. 39 (1938) 546.
[42] B.E. Deal, A.S. Grove, J. Appl. Phys. 36 (1965) 3770.
[43] J.P. Mardon, D. Charquet, J. Senevat, in: Proceedings of the 12th Symposium of the Zirconium in the Nuclear Industry, ASTM-STP 1295, American Society for Testing and Materials, 1998, p. 505.
[44] P. Bossis, J. Thomazet, F. Lefebvre, in: Proceedings of the 13th Symposium of the Zirconium in the Nuclear Industry, ASTM-STP 1295, American Society for Testing and Materials, 2001, p. 190.